Article

Control of Localized Nanorod Formation and Patterns of Semiconducting CuTCNQ Phase I Crystals by Scanning Electrochemical Microscopy

Aaron K. Neufeld, Anthony P. O'Mullane, and Alan M. Bond

J. Am. Chem. Soc., **2005**, 127 (40), 13846-13853• DOI: 10.1021/ja050561w • Publication Date (Web): 17 September 2005

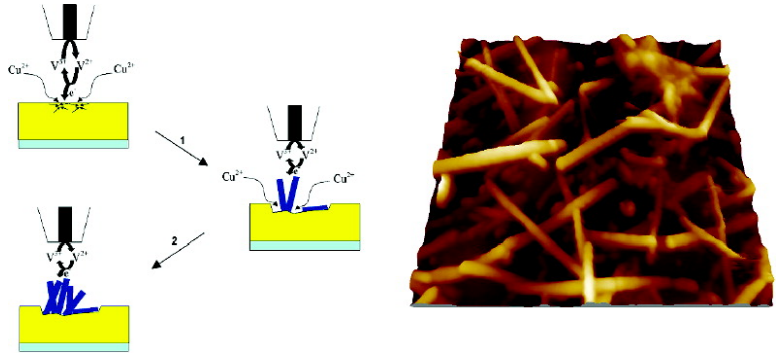

More About This Article

Additional resources and features associated with this article are available within the HTML version:

- Supporting Information
- Links to the 12 articles that cite this article, as of the time of this article download
- Access to high resolution figures
- Links to articles and content related to this article
- Copyright permission to reproduce figures and/or text from this article

View the Full Text HTML

J|A|C|S
ARTICLES
Published on Web 09/17/2005

Control of Localized Nanorod Formation and Patterns of Semiconducting CuTCNQ Phase I Crystals by Scanning Electrochemical Microscopy

Aaron K. Neufeld,*,† Anthony P. O'Mullane,‡ and Alan M. Bond*,‡

Contribution from the CSIRO Manufacturing and Infrastructure Technology, P.O. Box 56, Graham Road, Highett, Victoria 3190, Australia, and School of Chemistry, Monash University, Clayton, Victoria 3800, Australia

Received January 27, 2005; E-mail: Aaron.Neufeld@csiro.au; Alan.Bond@sci.monash.edu.au

Abstract: Use of the technique of scanning electrochemical microscopy (SECM) enables the surface of single crystals of 7,7′,8,8′-tetracyanoquinodimethane (TCNQ) to be modified in a controlled manner to produce highly dense and micrometer sized regions of semiconducting phase I CuTCNQ nanorod crystals by a nucleation and growth mechanism. This method involves the localized reduction of solid TCNQ to $TCNQ^-$ by aqueous phase $V^{2+}_{(aq)}$ reductant generated at a SECM ultramicroelectrode tip by reduction of $V^{3+}_{(aq)}$, coupled with the incorporation and reduction of $Cu^{2+}_{(aq)}$ ions also present in the aqueous electrolyte. SECM parameters can be systematically varied to control the extent of surface modification and the packing density of the CuTCNQ crystals. Scanning electron microscopy (SEM) and atomic force microscopy (AFM) images provide evidence that the TCNQ to CuTCNQ solid−solid transformation is accompanied by a drastic localized crystal volume and morphology change achieved by fragmentation of the TCNQ crystal surface. Patterns of semiconducting CuTCNQ (phase I) nanorod shaped crystals have been characterized by SEM, AFM, and infrared (IR) techniques. A reaction scheme has been proposed for the interaction between the electrogenerated mediator $V^{2+}_{(aq)}$, $Cu^{2+}_{(aq)}$, and the TCNQ crystal in the nucleation and growth stages of phase I CuTCNQ formation.

Introduction

Charge transfer complexes, coordination polymers, and organometallic complexes that have electronic properties, light harvesting ability, or both, are of considerable current interest. This is particularly true where these compounds take the form of nanoparticles, thin films, or self-assembled monolayers on a substrate that may be incorporated into a device for energy or information storage, catalysis, or sensing applications. Successful attempts to impart devices with such useful properties normally require a high level of control over various aspects of the functional moieties (phase, density, orientation, size, etc.) in addition to making them compatible with being integrated into conventional platforms, for which patterning is often desirable.

The attributes of tetracyanoquinodimethane (TCNQ) complexes have been researched for many years.[1] The copper−tetracyanoquinodimethane (CuTCNQ) charge transfer complex, which is of interest in this paper, has attracted much attention because of its intriguing structural, electronic, and optical properties.[2−6] Under appropriate experimental conditions, the nature of CuTCNQ formed can be controlled to give two distinct polymorphs, denoted as phase I and II, where these are the kinetically and thermodynamically favored phases, respectively.[5−7] However, CuTCNQ (phase I) is significantly more conducting, due to efficient π-stacking of the $TCNQ^{\bullet-}_{(s)}$ units. Opportunities for use of CuTCNQ phase I in the area of molecular electronics (e.g., optical data storage) requires a high level of control to ensure the proper phase is produced, and also an understanding of how very dense assemblies of pure CuTCNQ phase I material may be produced on the nanoscale size regime.

To date, methods of fabrication of CuTCNQ have been based on procedures, such as vapor deposition,[4] solution processes in organic solvents,[3,5,8] or chemical[5] and electrochemical reduction[7] of TCNQ in the presence of metallic Cu, Cu^+, or $Cu^{2+}_{(aq)}$ ions.

† CSIRO.
‡ Monash University.

(1) (a) Martin, N.; Segura, J. L.; Seoane, C. *J. Mater. Chem.* **1997**, *7*, 1661−1676. (b) Kaim, W.; Moscherosch, M. *Coord. Chem. Rev.* **1994**, *129*, 157−193. (c) Richard, J.; Delhaes, P.; Vandevyver, M. *New J. Chem.* **1991**, *15*, 137−148.
(2) (a) Potember, R. S.; Poehler, T. O.; Benson, R. C. *Appl. Phys. Lett.* **1982**, *41*, 548−550. (b) Sun, S. Q.; Wu, P. J.; Zhu, D. B. *Solid State Commun.* **1996**, *99*, 237−240. (c) Bond, A. M.; Symons, P. G.; Fletcher, S. *Analyst* **1998**, *123*, 1891−1904. (d) Kamna, M. M.; Graham, T. M.; Love, J. C.; Weiss, P. S. *Surf. Sci.* **1998**, *419*, 12−23. (e) Duan, H.; Cowan, D. O.; Kruger, J. *J. Electrochem. Soc.* **1993**, *140*, 2807−2815. (f) Huang, W. Q.; Wu, Y. Q.; Gu, D. H.; Gan, F. X. *Chin. Phys. Lett.* **2003**, *20*, 2178−2181.
(3) (a) Hoagland, J. J.; Wang, X. D.; Hipps, K. W. *Chem. Mater.* **1993**, *5*, 54−60. (b) Gu, N.; Zhang, H.-Q.; Wei, Y.; Shen, H.-Y.; Zhang, L. *Supramol. Sci.* **1998**, *5*, 691−693. (c) Sun, S.; Xu, X.; Wu, P.; Zhu, D. *J. Mater. Sci. Lett.* **1998**, *17*, 719−721.
(4) (a) Gu, N.; Yang, X.-M.; Sheng, H.-Y.; Lu, W.; Wei, Y. *Synth. Met.* **1995**, *71*, 2221−2222. (b) Wachtel, H.; Ohnmacht, M.; von Schuetz, J. U.; Wolf, H. C. *Nanostruct. Mater.* **1995**, *6*, 291−295. (c) Liu, S.-G.; Liu, Y.-Q.; Wu, P.-J.; Zhu, D.-B. *Chem. Mater.* **1996**, *8*, 2779−2787. (d) Oyamada, T.; Tanaka, H.; Matsushige, K.; Sasabe, H.; Adachi, C. *Appl. Phys. Lett.* **2003**, *83*, 1252−1254.
(5) Heintz, R. A.; Zhao, H.; Ouyang, X.; Grandinetti, G.; Cowen, J.; Dunbar, K. R. *Inorg. Chem.* **1999**, *38*, 144−156.
(6) Neufeld, A. K.; Madsen, I.; Bond, A. M.; Hogan, C. F. *Chem. Mater.* **2003**, *15*, 3573−3585.
(7) Harris, A.; Neufeld, A. K.; O'Mullane, A.; Bond, A. M.; Morrison, R. *J. Electrochem. Soc.* **2005**, *152*, C557−C583.

 10.1021/ja050561w CCC: $30.25

In the case of chemical methods of synthesis, the crystal size distribution is largely uncontrollable, while electrochemical synthesis involving the solid-state transformation of TCNQ to CuTCNQ is sensitive to TCNQ crystal size and the reproducibility of their adherence to an electrode surface.[6] Thus, existing methods have significant potential drawbacks with respect to controlling the size, phase, and morphology of CuTCNQ and lack the ability to achieve a patterning of structures.

In this paper, we introduce a new approach based on the use of the technique of scanning electrochemical microscopy (SECM) to address these limitations. The SECM method has been used in a variety of ways to induce surface modification[9] and offers the possibility of exhibiting a high level of control of the electrochemical component of the system and also provides potential for introduction of patterning capacities. To induce the solid-state conversion in an aqueous electrolyte requires unique experimental conditions to be established in which CuTCNQ phase I is formed by using a SECM electrogenerated mediator ($Med^{x+}_{(aq)}$) to reduce the surface of TCNQ in the presence of $Cu^{2+}_{(aq)}$ at the solid−liquid interface and in accordance with the generic reaction scheme

$$2Med^{x+}_{(aq)} + TCNQ_{(s)} + Cu^{2+}_{(aq)} \rightarrow 2Med^{(x+1)+}_{(aq)} + CuTCNQ_{(s)} \quad (1)$$

This strategy represents an innovative way to induce surface modification of solid compounds that are redox active, insulating, and are not in direct contact with an electrode material. Furthermore, by utilizing routine SECM modes (approach curves and constant height electrolysis), we demonstrate how control over the packing density and size of nanorod forms of CuTCNQ can be achieved, and also, possibilities for patterning of CuTCNQ regions within a single crystal of TCNQ now becomes available for the first time.

Experimental Section

Materials and Chemicals. Analytical grade VCl_3, 7,7′,8,8′-tetracyanoquinodimethane, propan-2-ol, acetone, and acetonitrile were used as received from Aldrich. All aqueous solutions were prepared from water (resistivity of 18.2 MΩ cm) purified by use of a Milli-Q reagent deionizer (Millipore).

Procedures. Glass substrates onto which TCNQ crystals were placed for probing by the SECM method were cleaned by sonication in acetone for 10 min, then in propan-2-ol before finally being dried by blowing with nitrogen. TCNQ single crystals were obtained from a supersaturated solution of TCNQ prepared by addition of TCNQ to a stirred boiling acetonitrile solution. Slow cooling led to the precipitation of TCNQ crystals, which were collected after a period of 3 days. Crystals of variable size were formed, but the large ones chosen for SECM experiments typically had dimensions of about 4 × 4 × 0.5 mm. Prior to each experiment, the selected crystal was rinsed with water to remove residual acetonitrile.

Cyclic voltammetric and SECM experiments were conducted with a CH Instruments, Model CHI 900 electrochemical analyzer. Voltammetry on TCNQ modified glassy carbon (GC) electrodes has been described previously.[6] SECM experiments were carried out with a two-electrode arrangement consisting of a 25 μm diameter Pt working electrode (UME) and a silver wire quasi-reference electrode (AgQRE). Repetitive SECM approach curves were obtained by relocating the UME to a new position on the TCNQ crystal (separation greater than 100 μm from the region of any previous measurement). Patterning of the TCNQ crystal was carried out by traversing the UME across the crystal at a constant tip−sample distance. Prior to all electrochemical experiments, the electrolyte was degassed using high purity argon. Infrared (IR), scanning electron microscopy (SEM), and visible light microscopy were performed using instrumentation and procedures described elsewhere.[6] Atomic force microscopy (AFM) images were obtained in tapping mode using a Digital Instruments Multimode AFM with Extender electronics and a Nanoscope IIIa controller.

Results and Discussion

Choice of a Suitable Mediator. The TCNQ to CuTCNQ solid−solid transformation when a TCNQ modified electrode is in contact with $Cu^{2+}_{(aq)}$ involves the overall reaction[6] summarized in eq 2.

$$TCNQ^{0}_{(s,GC)} + Cu^{2+}_{(aq)} + 2e^{-} \rightleftharpoons CuTCNQ_{(s)} \quad (2)$$

In the SECM form of an experiment designed to generate $CuTCNQ_{(s)}$ from $TCNQ_{(s)}$ and in the presence of aqueous $Cu^{2+}_{(aq)}$ electrolyte, the electrochemically reduced form of the mediator must have sufficient redox power to convert $TCNQ_{(s)}$ to $TCNQ^{\bullet-}_{(s)}$ only, and not further to $TCNQ^{2-}$. This experiment involves control of the UME potential only, with the TCNQ supported by an insulating material rather than an electrode surface. Since $Cu^{2+}_{(aq)}$ is present in the electrolyte, the mediator process must also occur in a potential window that avoids copper deposition at the UME. A mediator that fulfills these criteria is VCl_3, provided the $CuSO_4$ electrolyte concentration is sufficiently low.

Cyclic voltammograms obtained when 1 mM VCl_3 is reduced at a 25 μm diameter Pt UME in the presence of aqueous $CuSO_4$ electrolyte are illustrated in Figure 1a. Lowering the $CuSO_4$ electrolyte concentration from 0.1 to 0.01 M decreases the potential for onset of copper deposition from about 0.05 to −0.20 V. This allows the $V^{3+/2+}_{(aq)}$ process to occur at a less negative potential than for copper deposition, provided the potential is switched at ≤−0.20 V. Consequently, in all SECM experiments, 0.01 M $CuSO_4$ was used as the electrolyte, and the potential of the UME was held near the first of the $V^{3+/2+}_{(aq)}$ process at −0.07 ± 0.05 V. These conditions avoid copper deposition and provide a near steady-state current of 0.6 ± 0.05 nA at a 25 μm diameter UME.

The interplay between vanadium and copper ions also was established by cyclic voltammetric experiments. Figure 1b contains cyclic voltammograms at a TCNQ modified GC electrode in contact with 10 mM $CuSO_4$ (2nd and 20th cycles of the potential). In initial cycles, the overall reaction of $Cu^{2+}_{(aq)} + TCNQ^{0}_{(s)} + 2e^{-} \rightleftharpoons CuTCNQ_{(s)}$ (phase I) occurs. On extended potential cycling, the emergence of a second oxidation peak is associated with formation of the more thermodynamically stable phase II polymorph via the overall process $Cu^{2+}_{(aq)} + TCNQ^{0}_{(s)} + 2e^{-} \rightleftharpoons CuTCNQ_{(s)}$ (phase II). Mechanistic details are available in ref 6.

The voltammetry of a TCNQ modified electrode in the presence of $V^{3+}_{(aq)}$ (Figure 1b) is stable over the initial 20 cycles and represents a classic example of a nucleation and growth-

(8) (a) Liu, S.-G.; Liu, Y.-Q.; Zhu, D.-B. *Thin Solid Films* **1996**, *280*, 271−277. (b) Sun, S.; Wu, P.; Zhu, D. *Thin Solid Films* **1997**, *301*, 192−196.
(9) (a) Hess, C.; Borgwarth, K.; Ricken, C.; Ebling, D. G.; Heinze, J. *Electrochim. Acta* **1997**, *42*, 3065. (b) Ammann, E.; Mandler, D. *J. Electrochem. Soc.* **2001**, *148*, C533−C539. (c) Mandler, D.; Bard, A. J. *J. Electrochem. Soc.* **1990**, *137*, 1079−1086. (d) Macpherson, J. V.; Slevin, C. J.; Unwin, P. R. *J. Chem. Soc., Faraday Trans.* **1996**, *92*, 3799. (e) Marck, C.; Borgwarth, K.; Heinze, J. *Chem. Mater.* **2001**, *13*, 747. (f) Turyan, I.; Matsue, T.; Mandler, D. *Anal. Chem.* **2000**, *72*, 3431.

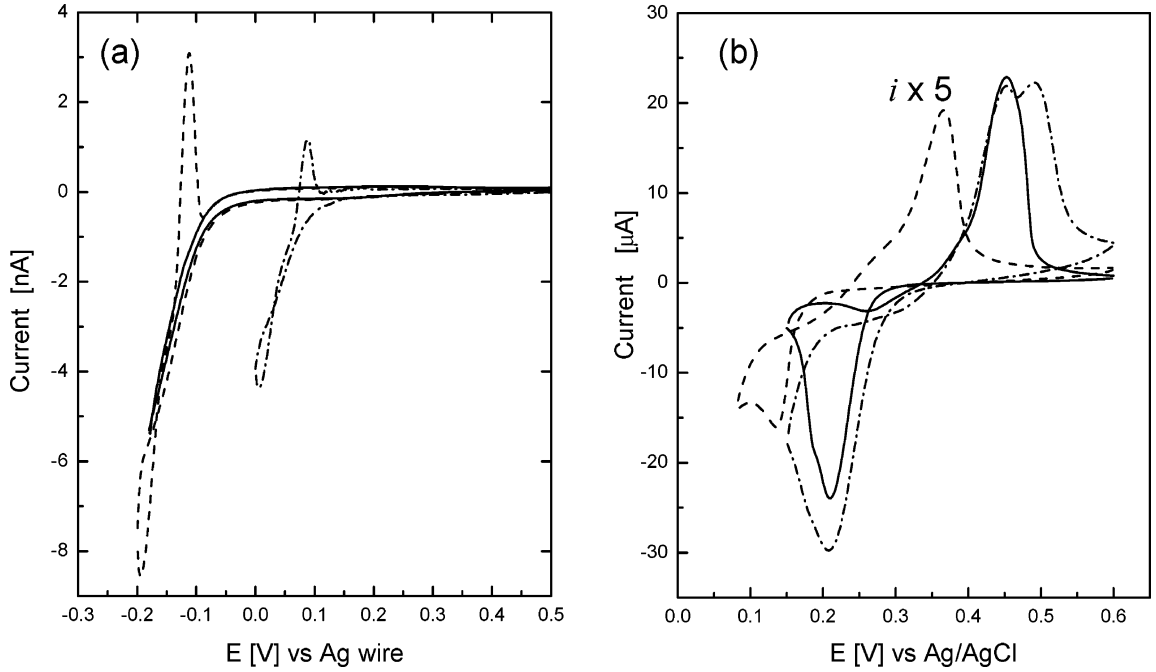

Figure 1. (a) Cyclic voltammograms obtained at a scan rate of 10 mV s^{-1} for reduction of 1 mM VCl_3 at a 25 μm Pt UME in the presence of 0.1 M $CuSO_4$ (-·-·-), 0.01 M $CuSO_4$ (- - -), and in the presence of 0.01 M $CuSO_4$ (—) when the potential is switched prior to the onset of the copper deposition process. (b) Cyclic voltammograms obtained at a scan rate of 20 mV s^{-1} when a GC electrode modified with microcrystals of TCNQ is placed in contact with aqueous electrolyte containing 0.01 M $CuSO_4$, 2nd (—) and 20th (-·-·-) cycle, or 1 mM VCl_3 (- - -).

type mechanism involving the formation of a vanadium−TCNQ complex. The mechanism has not been investigated in detail, but is tentatively assigned to the process:

$$V^{3+}_{(aq)} + 2TCNQ^{0}_{(s)} + 3e^{-} \rightleftharpoons [V^{2+}][TCNQ^{-}]_{2(s)} \qquad (3)$$

The voltammograms shown in Figure 1b also clearly reveal that formation of CuTCNQ occurs at a potential that is significantly more positive than that postulated for formation of $V[TCNQ]_2$. These data imply that formation of CuTCNQ is favored over that of vanadium complexes, as required in SECM experiments.

To confirm that vanadium insertion may be avoided, it was shown that cyclic voltammograms of a TCNQ modified GC electrode in contact with 0.01 M $CuSO_4$ electrolyte are indistinguishable in the presence or absence of 1 mM VCl_3 when a switching potential of 0.17 V was selected. Furthermore, IR data obtained on the solid present upon conversion from phase I to phase II exhibited the characteristic CuTCNQ (phase II) bands,[6] in both the presence and absence of $V^{3+}_{(aq)}$. Finally, elemental analysis by SEM (EDAX) of the solid obtained from the GC electrode after potential cycling experiments confirmed the presence of copper and the absence of vanadium. All these data imply that use of 1 mM VCl_3 as a mediator should lead to preferential formation of CuTCNQ. However, the electrogenerated form of the mediator $V^{2+}_{(aq)}$ could still be involved as an intermediate in the formation of CuTCNQ, as $V[TCNQ]_2$ is a known compound.[10]

Analysis of SECM Approach Curves. To establish that CuTCNQ can be generated on the surface of a TCNQ crystal under SECM conditions with a $V^{3+/2+}_{(aq)}$ mediator reaction, a series of approach curve experiments were undertaken that involved moving the UME at a constant rate toward the surface of the TCNQ crystal. At sufficiently close distance, it was anticipated that $TCNQ_{(s)}$ would be converted to $TCNQ^{\bullet-}_{(s)}$ by the electrogenerated mediator. If the $V^{3+}_{(aq)}$ is excluded from forming a new compound by the presence of $Cu^{2+}_{(aq)}$, it may then diffuse back to the UME and provide SECM feedback and, hence, facilitate positioning of the UME above the substrate. Figure 2 contains SECM approach curve data obtained at approach rates of 1 and 10 μm s^{-1}, respectively, with a 25 μm Pt UME held at −0.065 V vs AgQRE in the presence of aqueous electrolyte containing 1 mM VCl_3 and 0.01 M $CuSO_4$. In these experiments, translation of the UME was stopped prior to direct contact being made with the TCNQ surface. This was achieved by placing a limit on the maximum current ratio that would trigger the cessation of the UME translation process or stopping at a predetermined absolute position, relative to the TCNQ surface.

At an approach rate of 1 μm s^{-1} (Figure 2a), the first five approach curves made to the same location on the TCNQ surface display a small increase in maximum feedback ratio starting at a current ratio (i/i_{bulk}) of approximately 2.4. On the sixth approach, there is a marked increase in the feedback current up to $i/i_{bulk} = 4.5$. The seventh approach curve was almost the same as that of the sixth.

At a faster approach rate of 10 μm s^{-1} (Figure 2b), a more marked increase is detected in i/i_{bulk} ratio when successive approach curves are recorded. The first approach curve reaches a ratio of approximately 2.1. Approach curves 2−5 each increase by about 0.15. As with the approach curves at 1 μm s^{-1} described above, the sixth approach curve at 10 μm s^{-1} shows a marked increase in feedback, reaching a final ratio of about 3.5. Again, the seventh approach curves are indistinguishable from those of the sixth.

Standard methods for calculation of the heterogeneous electron transfer rates calculated from approach curve data[11]

(10) Vickers, E. B.; Selby, T. D.; Thorum, M. S.; Taliaferro, M. L.; Miller, J. S. *Inorg. Chem.* **2004**, *43*, 6414−6420.

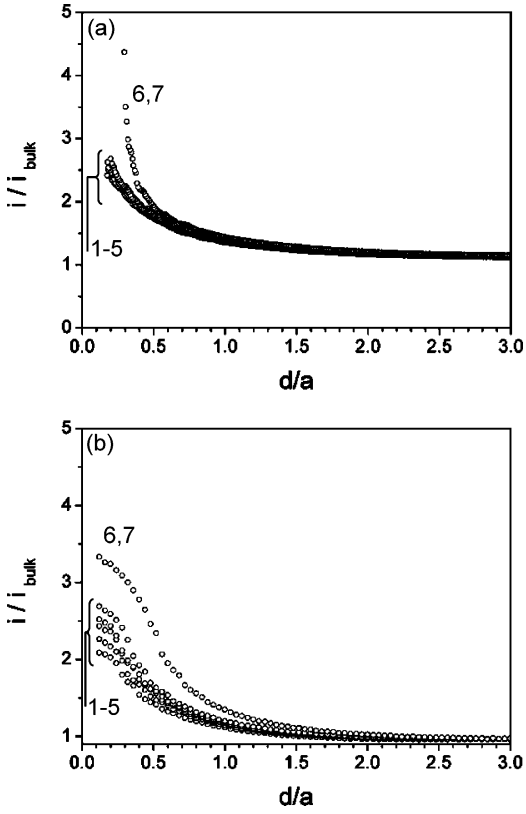

Figure 2. Approach curves representative of the first seven approach curve experiments obtained when a 25 μm Pt UME electrode held at −0.065 V vs Ag wire in 1 mM VCl_3 + 10 mM $CuSO_4$ has repetitively approached a TCNQ crystal at a rate of (a) 1 μm s^{-1} and (b) 10 μm s^{-1}. The current measured at the tip of the UME is *i*, and the current measured in the bulk solution is i_{bulk}; *d* is the tip−substrate separation, and *a* is the UME radius.

necessitate that a mediator be generated at a diffusion limited current and not induce surface modification. Such conditions apply when macroscopic samples of both phases of CuTCNQ are present on an insulating substrate when an innocent mediator is used.[12] However, detection of positive feedback in the present situation is consistent with progressive transformation of insulating TCNQ to semiconducting CuTCNQ during the course of each approach of the UME tip toward the TCNQ surface.

Inspection of the surface of a TCNQ crystal after approach curve experiments using a visible light microscope revealed blue circular regions that were close to the size of the UME diameter. However, resolution was not sufficient to establish the detail of any fine structure. With the aid of an IR microscope, principle IR absorption peaks observed at 2202 and 825 cm^{-1} confirm that these modified blue spots contained CuTCNQ phase I.

AFM and SEM Characterization of Modified TCNQ Surface. (a) Approach Curve Experiments at 1 μm s^{-1}. To obtain a better understanding of the SECM approach curve data (Figure 2), characterization by SEM and AFM was undertaken after approach curve experiments that involved one, three, and seven approaches to a single spot. SEM inspection of the TCNQ surface after a single approach at a rate of 1 μm s^{-1} revealed (Figure S1) a collection of crystals with needle shaped morphology indicative of CuTCNQ (phase I)[5,6] embedded in the TCNQ surface within a region slightly larger than the 25 μm UME tip

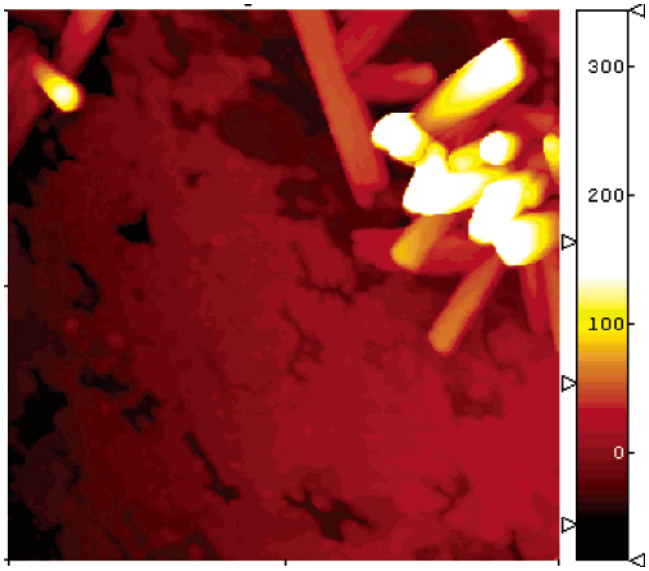

Figure 3. AFM height image of the surface of a TCNQ crystal that has been approached once by a 25 μm Pt UME electrode at a rate of 1 μm s^{-1}. Scan area = 2 × 2 μm, *z* range = 490 nm.

diameter. The nanorod-like crystals were typically between 300 and 700 nm in length and had length-to-width ratios of between 6 and 8 and formed small clusters, but there was typically between 1 and 2 μm of unmodified TCNQ surface surrounding them. Electron microprobe elemental analysis confirmed the presence of Cu within the rod shaped crystals (and the absence of vanadium).

Cavities exist in the surface of the TCNQ crystal in the region where CuTCNQ nanorod formation was investigated by tapping mode AFM experiments. The height image (Figure 3) shows evidence of a small degree of pitting in the unmodified areas of the TCNQ crystal (typical depths of 5−10 nm). However, in regions adjacent to the CuTCNQ nanorods, cavities with depths of up to 100 nm are detected. TCNQ and CuTCNQ (phase I) have densities (unit cell volumes) of 1.34 g cm^{-3} (1030.8 $Å^3$) and 1.80 g cm^{-3} (493.5 $Å^3$), respectively.[5] This outcome is consistent with drastic density and cell volume changes required to convert TCNQ to CuTCNQ in addition to the change in crystal habit. Severe fragmentation of TCNQ crystals when CuTCNQ is formed is also observed by potential cycling and potential step experiments under conditions where TCNQ crystals adhered to a GC electrode in contact with aqueous $CuSO_4$ electrolyte.[6]

The extent of SECM feedback increases marginally when the UME approaches the TCNQ surface at a rate of 1 μm s^{-1} on occasions 2 to 4 (Figure 2a). SEM micrographs (Figure S2) reveal that upon three approaches, the intensity of surface modification has increased in comparison to that of a single approach experiment. In particular, the density of nanorods has increased substantially, but not the size of the nanorods. Interestingly, the majority of the CuTCNQ rods are the same size with lengths between 800 and 1000 nm and an aspect ratio about 10:1. Clusters of CuTCNQ crystals remain somewhat isolated from each other, and the extensive cavitation around the CuTCNQ needles seen after a single approach curve experiment is no longer as evident. These observations can be accounted for by assuming that the growth of CuTCNQ in the second and third approaches fills the voids formed during the

(11) Kwak, J.; Bard, A. J. *Anal. Chem.* **1989**, *61*, 1221−1227.
(12) O'Mullane, A.; Neufeld, A. K.; Bond, A. M. *Anal. Chem.* **2005**, *17*, 5447−5452.

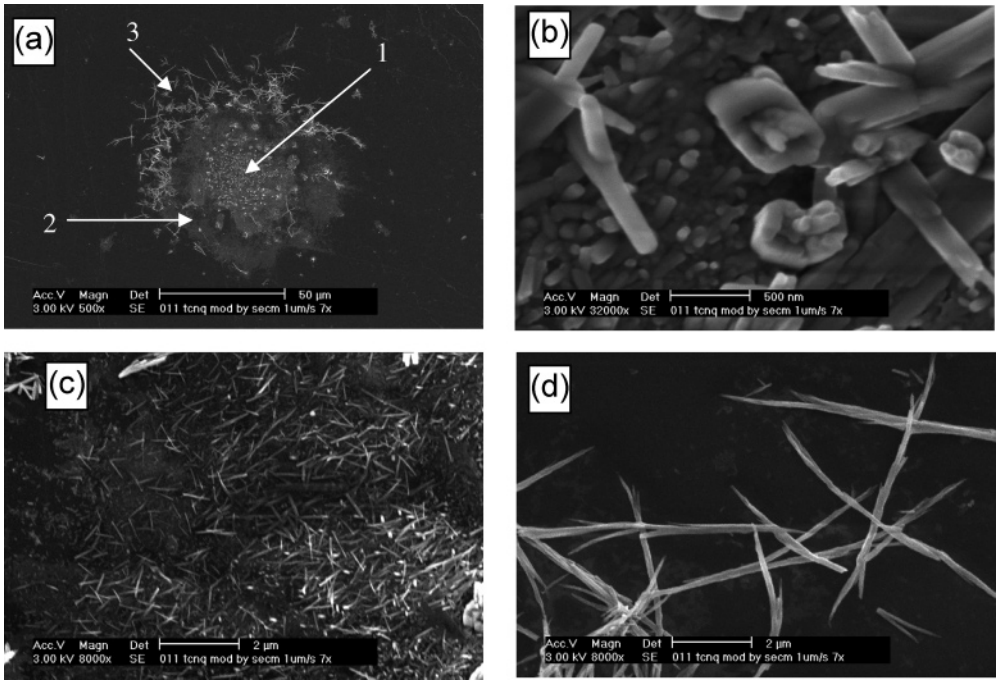

Figure 4. SEM micrographs obtained after a TCNQ crystal has been approached seven times at a rate of 1 μm s^{-1} by a 25 μm Pt UME electrode held at -0.065 V vs Ag wire in 1 mM VCl_3 + 10 mM $CuSO_4$. (a) Entire region. Subregions 1, 2, and 3 of (a) are shown at higher magnification in images in b, c, and d, respectively.

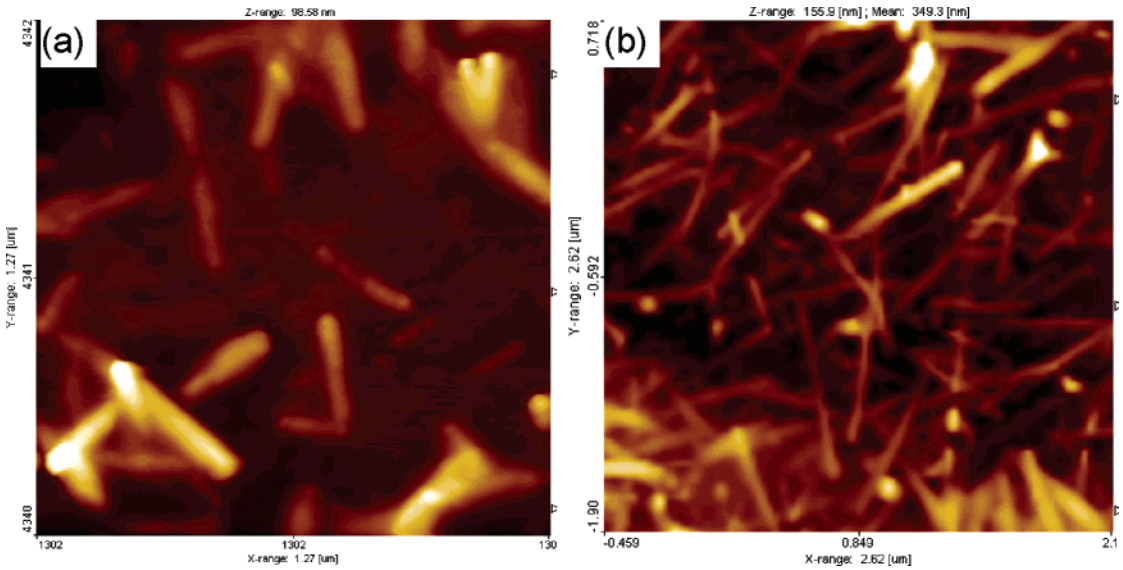

Figure 5. Tapping mode AFM height images obtained from region 2 as indicated in Figure 4c. Scan dimensions are (a) 1.2 $\times$ 1.27 μm with z range of 98.5 nm, and (b) 2.62 $\times$ 2.62 μm with z range of 156 nm.

initial surface modification, in addition to increasing the size of the smaller crystals.

The extent of SECM positive feedback increased considerably in the sixth approach experiment (Figure 2a). Evaluation of SEM images after the seventh approach curve (Figure 4) reveals that this can be attributed to the fact that the UME now approaches an almost continuous assembly of semiconducting CuTCNQ nanorods. That is, the packing density has now increased so dramatically that the CuTCNQ crystals are now in intimate contact with each other and may act as a highly conducting network.[12] The central region (labeled 1) is comparable in size to the 25 μm diameter of the UME and consists of densely packed CuTCNQ crystals that grow in both the parallel and perpendicular directions to the original flat TCNQ crystal surface (Figure 4b). A second region (labeled 2) consists of a band of much smaller crystals that are densely packed together but oriented randomly. Their morphology was better determined using AFM, primarily because electron beam induced charging of the underlying TCNQ crystal base obscured the resolution of these nanometer sized features. AFM images (Figure 5 and Figure S3) taken at different areas within region 2 consists of $<$500 nm long CuTCNQ crystals with an aspect ratio of 6$-$8. A gradual decrease in CuTCNQ crystal packing density that occurs when traversing from the inner to the outer edge of region 2 is accompanied by the presence of cavitation, as observed previously in earlier approach curve experiments. The third region (labeled 3) lies at the perimeter of the modified TCNQ region and consists of very long CuTCNQ crystals, up to 5 μm

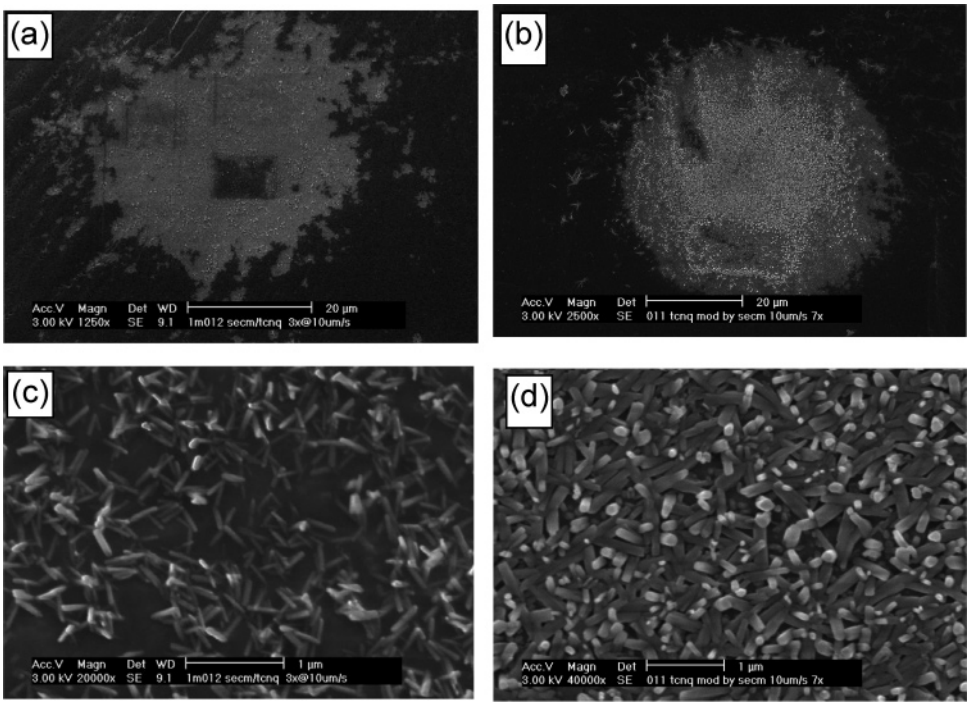

Figure 6. SEM images obtained after a TCNQ crystal has been approached at a rate of 10 μm s^{-1} by a 25 μm Pt UME electrode held at −0.065 V vs Ag wire under SECM conditions. (a and c) Three repetitive approaches, and (b and d) after seven repetitive approaches.

in length. Figure 4d is a high-magnification SEM image of these nanowire crystals.

The presence of a region of substantial CuTCNQ formation (region 3) outside that of the 25 μm diameter of the UME tip suggests that a nucleation−growth mechanism is operative. Regions 1 and 2 are derived from direct interaction of $V^{2+}_{(aq)}$ formed within the diffusion field of the mediator and the TCNQ crystal. The flux of reduced mediator was generated by predominately linear diffusion in the central region of the microelectrode, with an edge or radial diffusion being dominant at the perimeter. The manifestation of this is illustrated by the AFM height images in Figures 5 and S3. Since CuTCNQ (phase I) is semiconducting, electrons may propagate along CuTCNQ formed from previous approaches and reduce TCNQ that is in intimate contact with the already formed CuTCNQ, thereby providing a growth pathway for CuTCNQ nanorods. This nucleation−growth mechanism would explain the higher density of small, connected TCNQ crystals formed in region 2 and also how CuTCNQ can grow in the perpendicular direction to the underlying TCNQ crystal. Consistent with this model, the larger crystals formed at the outermost region 3 are the result of nucleation sites that grow into a region where TCNQ is readily available.

(b) Approach Curve Experiments at 10 μm s^{-1}. The above observations all refer to a UME approach rate of 1 μm s^{-1}. Use of a much faster approach rate of 10 μm s^{-1} gives rise (Figure 2b) to a more gradual increase in the positive feedback effect. Each curve is now associated with a small change in the size, but large change in density of CuTCNQ nanorods (Figure 6a−d). (The rectangular feature visible in Figure 6a is the result of electron beam irradiation at a higher magnification and accelerating voltage.) At 3 and 7 repetitive approaches at the faster rate, the modified TCNQ region is now much more confined to the area of the UME, and also is composed of smaller CuTCNQ crystals with a much higher packing density (comparing Figure 6c and S2). Thus, the CuTCNQ crystals are in more intimate contact with each other and so provide a more continuous conducting network of CuTCNQ, which amplifies the SECM positive feedback effect in each approach experiment. The increased rate also provides less time for the edge diffusion effect to generate nucleation sites in a region that enables them to grow to larger crystals. However, a low-density region of relatively larger CuTCNQ crystals is still formed at the outermost edge of the modified TCNQ crystal area.

In summary, use of an increased UME approach rate results in greater confinement of the CuTCNQ region and formation of smaller and more densely packed rod shaped crystals oriented perpendicular to the TCNQ surface (typical length 200−500 nm). The area of CuTCNQ formation extends beyond the 25 μm UME diameter, and the greater number of CuTCNQ crystals growing perpendicular to the TCNQ crystal support the importance of a growth mechanism following a nucleation process.

(c) Constant Height Electrolysis. To emphasize the versatility of TCNQ surface modification that may be achieved by the SECM method, the UME was held over different locations of a TCNQ crystal at known distances and different periods of time. Figure S4 illustrates the outcome in the form of SEM images for electrolysis experiments using time−height combinations of 30 s at 1.7 μm and 60 s at 5.0 μm. This result is analogous to when fast approach rates of the UME to the crystal surface are employed (10 μm s^{-1}). With respect to the 30 s at 1.7 μm case, despite a closer UME−surface proximity than for the 60 s at 5 μm conditions, significantly smaller crystals are detected with the shorter electrolysis period. This implies that the 250 μm diameter glass sheath on the UME restricts the diffusion of $Cu^{2+}_{(aq)}$ to the region where $V^{2+}_{(aq)}$ comes into contact with the surface and directly affects CuTCNQ growth. This is

consistent with the "hindered diffusion" effect observed in analytical uses of the SECM.[11]

The ability to micropattern a TCNQ crystal with semiconducting CuTCNQ (phase I) over large lengths of its surface was demonstrated by examining SEM images obtained after scanning the UME laterally across a TCNQ crystal. Figure S5 illustrates the formation of a 100 μm line of CuTCNQ when the UME tip is moved over the surface at a rate of 0.1 μm s^{-1}. A dense area of highly aligned CuTCNQ is present, where the UME initially was positioned, and corresponds to the place (see Figure S5b) at the bottom of the micrograph S5a. A well-defined region where TCNQ has been converted to CuTCNQ is detected when scanning occurs over a length of the surface. In this scanning regime, the density of the crystals is lower, but the size of the crystals formed is larger (see Figure S5c) than seen in approach curve experiments. At scan rates of greater than 10 μm s^{-1}, very little conversion of TCNQ to CuTCNQ is detected in SEM images. It is deduced from these and other data that the growth component of the mechanism to form needles of CuTCNQ (phase I) requires that a continual supply of $V^{2+}_{(aq)}$ needs to be both generated at the UME and also be accessible to the TCNQ surface.

A variation of the line modification method involved mapping a 300 × 300 μm area by rastering the UME across the TCNQ crystal in 5 μm increments at a scan rate of 25 μm s^{-1} (when a 25 μm Pt UME is used under these conditions, there is a repetitive exposure of the crystal with each traverse). This procedure gives rise to the visible light and SEM images presented in Figure S6. In the visible light microscope image, regions of blue colored CuTCNQ are clearly visible on the amber colored TCNQ single crystal. In this type of experiment, a significant level of conversion is achieved even with fast scan rates of 25 μm s^{-1}.

The outcome of the rastering experiment importantly demonstrates the interplay between lateral scan rate and the growth mechanism for CuTCNQ. By the nature of the modification of TCNQ to CuTCNQ, nucleation sites are initially created at minute defects or cracks present in the TCNQ crystal. Crystal growth can occur at these nucleation sites when V^{2+} is made available by the UME. This enables CuTCNQ formation at high scan rates in rastering experiments possible, noting that the nanorods were not detected in a single linear scan experiment at a rate of 10 μm s^{-1}.

These patterning experiments demonstrate that an advantage of the SECM experiment relative to direct electrochemical synthetic methods is that surface modification results solely from homogeneous charge transfer. Consequently, the nature and region of the surface modification can be controlled by the SECM electrode geometry, rate of electrode approach to the TCNQ surface, and the number of times the surface is approached, or by lateral scan rate and tip−surface separation. Additionally, nonmodified regions of a TCNQ crystal may be retained.

Mechanism and Related Aspects of the SECM Induced Transformation. In electrochemical studies on the solid−solid interconversion of TCNQ to CuTCNQ, formation of a transient species $[Cu^{2+}TCNQ^{\bullet-}]^{+}_{(transient)}$ at the solid−electrolyte interface was postulated.[6] In the SECM experiment, there is no underlying electrode in direct contact with TCNQ to provide electrons. Thus, if an analogous mechanism is operative, then the flux of $V^{2+}_{(aq)}$ generated at the UME (eq 4) must be used as a source of electrons. On this basis, a reaction scheme of the kind given in eqs 4−7 (net reaction in eq 7) can be proposed.

$$V^{3+}_{(aq)} + e^{-} \xrightarrow{UME} V^{2+}_{(aq)} \quad (4)$$

$$V^{2+}_{(aq)} + Cu^{2+}_{(aq)} + TCNQ_{(s)} \rightarrow V^{3+}_{(aq)} + [Cu^{2+}TCNQ^{\bullet-}]^{+}_{(transient)} \quad (5)$$

$$[Cu^{2+}TCNQ^{\bullet-}]^{+}_{(transient)} + V^{2+}_{(aq)} \rightarrow Cu^{+}TCNQ^{\bullet-}_{(s)} + V^{3+}_{(aq)} \quad (6)$$

$$2V^{2+}_{(aq)} + Cu^{2+}_{(aq)} + TCNQ_{(s)} \rightarrow 2V^{3+}_{(aq)} + Cu^{+}TCNQ^{\bullet-}_{(s)} \quad (7)$$

The involvement of a $V[TCNQ]_2$ intermediate is also likely (eq 8), given that this is a readily formed and stable material.[10] The vanadium compound would then have to undergo a site exchange with the $Cu^{2+}_{(aq)}$ ions present in solution (eq 9). This process in addition to that in eqs 5 and 6 also liberates $V^{3+}_{(aq)}$ ions, which would diffuse back to the UME and participate in the feedback effect observed in the approach curves (Figure 3).

$$3V^{2+}_{(aq)} + 2TCNQ_{(s)} \rightarrow 2V^{3+}_{(aq)} + [V^{2+}][TCNQ^{-}]_{2(s)} \quad (8)$$

$$Cu^{2+}_{(aq)} + [V^{2+}][TCNQ^{-}]_{2(s)} \rightarrow V^{3+}_{(aq)} + TCNQ^{\bullet-}_{(aq)} + [Cu^{+}][TCNQ^{\bullet-}]_{(s)} \quad (9)$$

Figure 7 summarizes the manner in which the SECM technique is applied in the present study. Initially, the SECM ultramicroelectrode approaches the surface of the TCNQ crystal (Figure 7a). The potential applied to the UME allows the $V^{3+}_{(aq)}$ mediator to be reduced to $V^{2+}_{(aq)}$, which induces (step 1) the chemical formation of CuTCNQ in the localized part of the TCNQ surface (Figure 7b) via the overall reaction given in eq 7. As the UME approaches the surface, or as the electrolysis time increases (step 2), the extent of surface modification may increase (Figure 7c), provided the growth phase is not limited by the absence of $V^{2+}_{(aq)}$ or $Cu^{2+}_{(aq)}$. The current change detected by the recycling of $V^{2+/3+}_{(aq)}$ is governed by the TCNQ surface−UME tip separation.

Conclusions

The SECM method can be employed with a $V^{2+/3+}_{(aq)}$ mediator and $Cu^{2+}_{(aq)}$ electrolyte to modify the surface of a TCNQ crystal in a controlled manner with the production of semiconducting CuTCNQ (phase I) nanorods of variable size and packing density. The large crystal volume changes that occur when the surface of virgin TCNQ is transformed to CuTCNQ, intrinsically leads to fragmentation of the surface of the mother crystal. Upon more extensive conversion, these initially fragmented areas become filled to achieve a densely packed film of semiconducting CuTCNQ in the area approached by the UME probe. Because the mechanism of CuTCNQ formation involves a nucleation−growth mechanism, the growth stage and hence the packing density and size of CuTCNQ crystals can be controlled by the nature of the approach of the UME toward the TCNQ crystal surface. Thus, a high rate of approach restricts the extent of conversion and increases the packing density by generation of smaller CuTCNQ crystals relative to that achieved with a slow approach rate. A related effect can also be achieved by

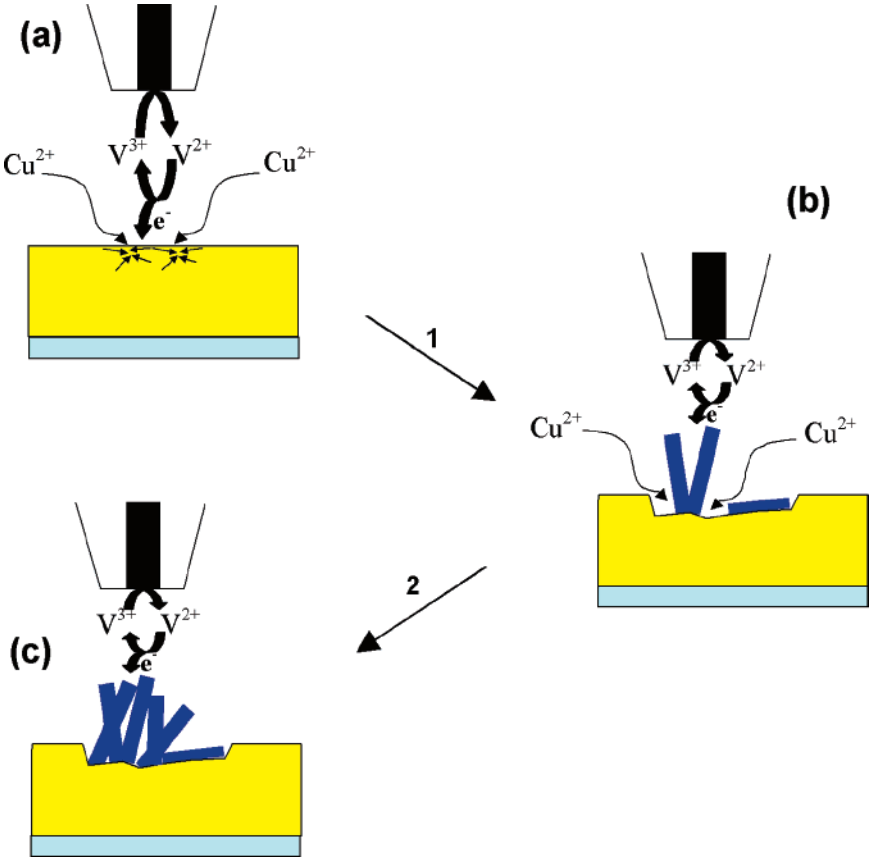

Figure 7. Schematic diagram illustrating the formation of CuTCNQ by the SECM technique. Step 1 (a → b) involves initial formation of CuTCNQ. Step 2 (a → b) involves further growth of CuTCNQ. (c) Indicates the final end state of the experiment. For convenience, the relative CuTCNQ nanorod shaped crystals to SECM UME size has been drawn at a scale of about 1:200.

positioning the UME at a fixed distance above the TCNQ crystal. In this case, continuous generation of $V^{2+}_{(aq)}$ occurs to produce highly confined areas of CuTCNQ nanorods and nanowires. It is also possible to micropattern a TCNQ crystal and vary the size and density of CuTCNQ nanosized rod shaped crystals. A rastering procedure provides another method of achieving control over the extent of conversion and crystal size. The SECM technique, therefore, provides the possibility of fabricating densely packed arrays of small semiconducting CuTCNQ crystals (<500 nm in length), and perhaps other compounds that may be of technological interest as part of a device for energy or information storage, catalysis, or sensing applications.

Acknowledgment. The authors express their appreciation to Dr. V. Gutowski for insightful comments, and Dr. L. Kolarik and J. Ward for technical assistance with AFM and SEM instrumentation, respectively. Financial support by CSIRO division of Manufacturing and Infrastructure Technology and the Australian Research Council is also gratefully acknowledged.

Supporting Information Available: Additional SEM and AFM images (Figure S1−S6) of TCNQ crystals converted to CuTCNQ by SECM based approach curve, constant height electrolysis, and rastering experiments. This material is available free of charge via the Internet at http://pubs.acs.org.

JA050561W